Consistency of Non-Double-Couple Components of Seismic Moment Tensors with Earthquake Magnitude and Mechanism

Boris Rösler[*1] and Seth Stein[1,2]

Abstract

Earthquake moment tensors can be decomposed into double-couple components describing slip on planar faults and non-double-couple (NDC) components. NDC components can arise in three ways. Some appear to be intrinsic, indicating complex source processes differing from slip on a fault for earthquakes in specific geologic environments, notably volcanic areas. Others are additive, reflecting the combined effect of double-couple sources on multiple faults with different geometries. Alternatively, they may be artifactual, results of the inversion without geologic meaning. Combining moment tensors from three global and four regional catalogs for 2016–2020 provides a dataset of NDC components of 12,856 earthquakes with $2.9 < M_w < 8.2$ in various geologic environments. The distributions of NDC components vary only slightly with magnitude, with a mean deviation from a double-couple source of around 20%. The consistency suggests that most NDC components do not reflect rupture on multiple faults, which is expected only for larger earthquakes. Similarly, there are only small differences in NDC components between earthquakes with different faulting mechanisms or in different geologic environments. These consistencies suggest that most NDC components are not intrinsic due to complex source processes that are often assumed to be most likely in volcanic and thus extensional areas. Hence, it appears that for most earthquakes, especially smaller ones, the NDC components are largely artifacts of the inversion.

Cite this article as Rösler, B., and S. Stein (2022). Consistency of Non-Double-Couple Components of Seismic Moment Tensors with Earthquake Magnitude and Mechanism, *Seismol. Res. Lett.* **XX**, 1–14, doi: 10.1785/0220210188.

Supplemental Material

Introduction

The deployment of digital seismic networks allowed determination of earthquake moment tensors, which describe components of the source beyond a double-couple (DC) force system representing slip on a fault plane (Gilbert, 1971). As catalogs of moment tensors were developed (Dziewonski and Woodhouse, 1983), it became clear that many earthquakes showed non-double-couple (NDC) components whose origin became a topic of investigation (Sipkin, 1986; Frohlich, 1994; Julian *et al.*, 1998; Miller *et al.*, 1998).

An NDC component is identified by decomposing a moment tensor. Diagonalization yields a tensor with eigenvalues λ_1, λ_2, and λ_3 on its diagonal, where $\lambda_1 > \lambda_3 > \lambda_2$. Subtracting a diagonal matrix with components equal to the isotropic moment $M_0^{iso} = (\lambda_1 + \lambda_2 + \lambda_3)/3$, representing the source's volumetric change, yields the deviatoric moment tensor typically reported in catalogs. This has no net volume change, because its trace, the sum of its eigenvalues, $\lambda_1' + \lambda_2' + \lambda_3' = 0$.

The deviatoric moment tensors found by inversions typically have three nonzero eigenvalues. Most have $\lambda_1' \approx -\lambda_2'$ and $|\lambda_1'| \gg |\lambda_3'|$. For a pure double couple, $\lambda_3' = 0$ and $\lambda_1' = -\lambda_2'$. If λ_3' is nonzero, the deviatoric tensor is decomposed into DC and NDC components.

This decomposition is not unique. One is into major (MDC) and minor (mDC) double couples (Kanamori and Given, 1981), each with equal and opposite eigenvalues,

$$\begin{pmatrix} \lambda_1' & 0 & 0 \\ 0 & \lambda_2' & 0 \\ 0 & 0 & \lambda_3' \end{pmatrix} = \begin{pmatrix} \lambda_1' & 0 & 0 \\ 0 & -\lambda_1' & 0 \\ 0 & 0 & 0 \end{pmatrix} + \begin{pmatrix} 0 & 0 & 0 \\ 0 & -\lambda_3' & 0 \\ 0 & 0 & \lambda_3' \end{pmatrix}. \quad (1)$$

1. Department of Earth and Planetary Sciences, Northwestern University, Evanston, Illinois, U.S.A., https://orcid.org/0000-0001-8596-5650 (BR); https://orcid.org/0000-0003-0522-7418 (SS); 2. Institute for Policy Research, Northwestern University, Evanston, Illinois, U.S.A.

*Corresponding author: boris@earth.northwestern.edu

Typically, $|\lambda_1'|$ is much larger than $|\lambda_3'|$, so the major double couple is treated as the earthquake's source mechanism, and the minor double couple is considered the NDC component.

Another decomposition (Knopoff and Randall, 1970) describes the NDC component as a compensated linear vector dipole (CLVD), three force dipoles with one twice the magnitude of the others, yielding no volume change,

$$\begin{pmatrix} \lambda_1' & 0 & 0 \\ 0 & \lambda_2' & 0 \\ 0 & 0 & \lambda_3' \end{pmatrix} = (\lambda_1' + 2\lambda_3') \begin{pmatrix} 1 & 0 & 0 \\ 0 & -1 & 0 \\ 0 & 0 & 0 \end{pmatrix} + \lambda_3' \begin{pmatrix} -2 & 0 & 0 \\ 0 & 1 & 0 \\ 0 & 0 & 1 \end{pmatrix}. \quad (2)$$

The polarity of λ_3' indicates whether there are two axes of compression and one of dilatation or the opposite.

The scalar moments of the MDC and the NDC (mDC or CLVD) differ between the decompositions. However, for either decomposition, the ratio of the smallest and the absolutely largest eigenvalues $\epsilon = \lambda_3'/\max(|\lambda_1'|, |\lambda_2'|)$ quantifies the size of the NDC component, the deviation from a DC source (Dziewonski *et al.*, 1981).

The different decompositions reflect the fact that the moment tensor describes a force system, so both decompositions reflect the same net force system and thus generate the same seismic waves. Hence, the seismic waves alone cannot distinguish between alternative decompositions.

Origin of NDC Components

Since the recognition that many earthquakes' moment tensors have NDC components, three general processes have been identified. Some appear to reflect intrinsically complex source processes that differ from slip on a planar fault for earthquakes in specific geologic environments, notably volcanic areas. Others arise from the combined effect of DC sources with different geometries or artifacts of the inversion process used to find the moment tensor from the seismograms. In some cases, several of these may have occurred. In this article, we denote source processes as complex only if they have intrinsic NDC components, although multifault ruptures are often also described as complex source processes.

We examine a large dataset of moment tensors to assess the relative role of these processes. We do this by considering characteristics of the three processes, based on previous studies of specific earthquakes.

Intrinsic NDC components

NDC components of moment tensors can be intrinsic, resulting from components of the source beyond slip on a planar fault. These are often reported in volcanic environments, as in the examples in Figure 1a. The 1980 eruption of Mount St. Helens generated seismic waves whose moment tensor has a 36% NDC component, which Kanamori and Given (1982) modeled as an almost horizontal single force. Julian (1983) modeled an M_w 6.2 event with a 61% NDC component that occurred in 1980 near the Long Valley Caldera in California as due to magma inflating a northwest-trending magma dike. The corresponding CLVD has a horizontal principal extensional axis trending northeast. Nettles and Ekström (1998) observed CLVD components of up to 83% for ten shallow earthquakes at Bárdarbunga volcano in Iceland and interpreted them as due to slip on an outward-dipping cone-shaped ring fault associated with inflation of a shallow magma chamber. In all these cases, the mechanism shown is that corresponding to the deviatoric moment tensor reported in catalogs, which excludes the actual source's isotropic component. The larger the NDC components, the more these mechanisms differ from the familiar focal mechanisms with perpendicular nodal planes indicating a DC source.

These examples illustrate various ways that intrinsic NDC components can arise. Figure 2, after Hudson *et al.* (1989), shows a useful conceptualization of source types and corresponding force systems in a plot with constant probability density. The horizontal coordinate

$$T \equiv 2\epsilon = \frac{2\lambda_3'}{\max(|\lambda_1'|, |\lambda_2'|)} \quad (3)$$

describes the relative sizes of the DC and CLVD components, whereas the vertical coordinate

$$k \equiv \frac{M_0^{\text{iso}}}{\max(|\lambda_1'|, |\lambda_2'|)} \quad (4)$$

measures the volume change. DC sources, representing slip on a fault with no volume change or deformation at the hypocenter lie in the center of the plot. Seismic sources including CLVDs, but without volume change, form the x-axis of the plot. Hence, the deviatoric solutions in moment tensor catalogs lie on this axis. Moment tensors that include both an isotropic component and a CLVD component are atypical seismic events whose radiation of seismic waves differs from those of earthquakes on planar faults. As in Figure 1, the mechanisms shown for the Mount St. Helens eruption and 1980 Long Valley event are those without an isotropic component, but negative CLVD component, representing the opening of a crack.

Additive NDC components

NDC components can arise from near-simultaneous earthquakes on nearby faults of different geometries (e.g., Julian and Sipkin, 1985; Wallace, 1985; Sipkin, 1986; Kawakatsu, 1991; Hayes *et al.*, 2010; Cirella *et al.*, 2012; Hamling *et al.*, 2017). This effect is consistent with the fact that the NDC component can be described as an mDC.

Figure 1b shows examples involving earthquakes with subevents. Scognamiglio *et al.* (2018) found slip on two faults during the M_w 5.6 earthquake near Norcia, Italy in 2016. Normal faulting on both faults yielded a moment tensor with

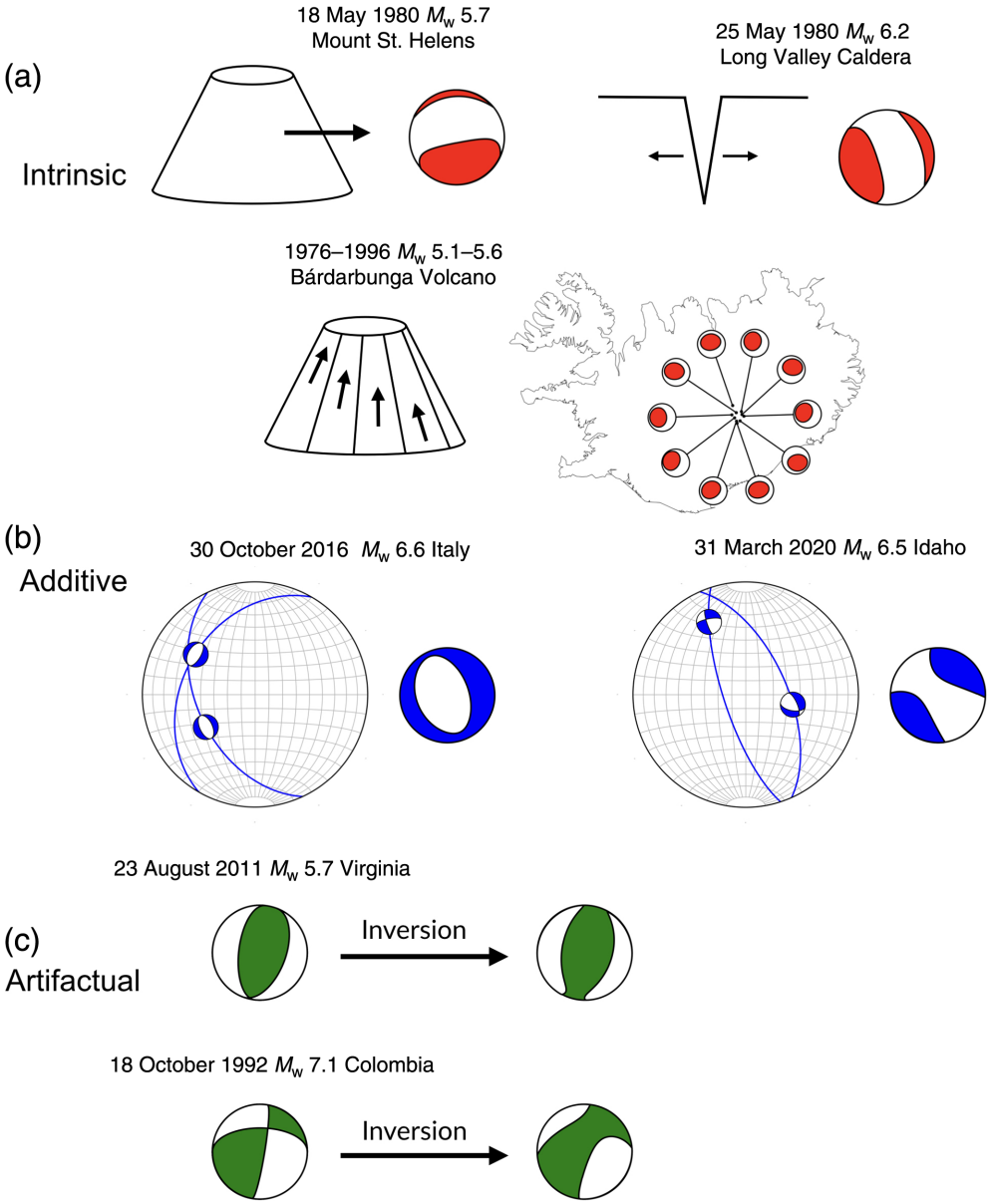

Figure 1. Causes of non-double-couple (NDC) components. (a) Intrinsic NDC components for the Mount St. Helens eruption, a dyke inflated by magma intrusion in the Long Valley Caldera, and earthquakes at Bárdarbunga Volcano. (b) Additive NDC components for earthquakes with slip on multiple faults: an earthquake in Italy with two faults with different strikes and an earthquake in Idaho with different mechanisms on two faults. (c) Artifactual NDC components resulting from the inversion, giving an apparent NDC component for earthquakes with a simple rupture geometry in Virginia and Colombia. The color version of this figure is available only in the electronic edition.

the mechanism shown and a NDC component of 15%. The 2020 M_w 6.5 earthquake near Stanley, Idaho, involved slip with different mechanisms on two intersecting faults, resulting in a 43% NDC component (Yang *et al.*, 2021).

Artifactual NDC components

NDC components can also arise as artifacts of the moment tensor inversion (Fig. 1c). Slip during the 23 August 2011 Virginia earthquake occurred on one fault, which coincides with the location of aftershocks (Chapman, 2013; McNamara *et al.*, 2014). However, the inversion results in a 10% NDC component, which seems likely to be an artifact. Seismic waves of the 18 October 1992 earthquake in Colombia reflect near-source propagation effects, resulting in a NDC component of 44%, whereas an inversion based on empirical Green's functions reveals a simple rupture geometry (Ammon *et al.*, 1994).

Seismograms are a linear combination of Green's functions weighted by the components of the moment tensor. Hence, artifacts can arise in the inverse problem by finding the best fit to the data, given assumed Green's functions. The moment tensor components and hence the NDC component depend on specific aspects of the inversion process including the parts of the wave field inverted, the model for elastic and anelastic Earth structure assumed (Šílený, 2004; Cesca *et al.*, 2006, Rößler *et al.*, 2007), noise in the data (Šílený *et al.*, 1996; Jechumtálová and Šílený, 2001), and the number and azimuthal coverage of seismic stations used (Cesca *et al.*, 2006; Ford *et al.*, 2010; Vera Rodriguez *et al.*, 2011; Domingues *et al.*, 2013). For example, Tréhu *et al.* (1981) found that NDC mechanisms on the Mid-Atlantic Ridge, recognized from nonorthogonal fault planes in focal mechanisms, arise because of noise in the data and two moment tensor components that are poorly resolved for shallow earthquakes, because the relevant stress eigenfunction and hence excitation coefficient goes to zero at the surface.

Distinguishing NDC components

Determining which of the three processes caused the NDC component associated with a given earthquake is challenging. In most cases, NDC components are often implicitly assumed

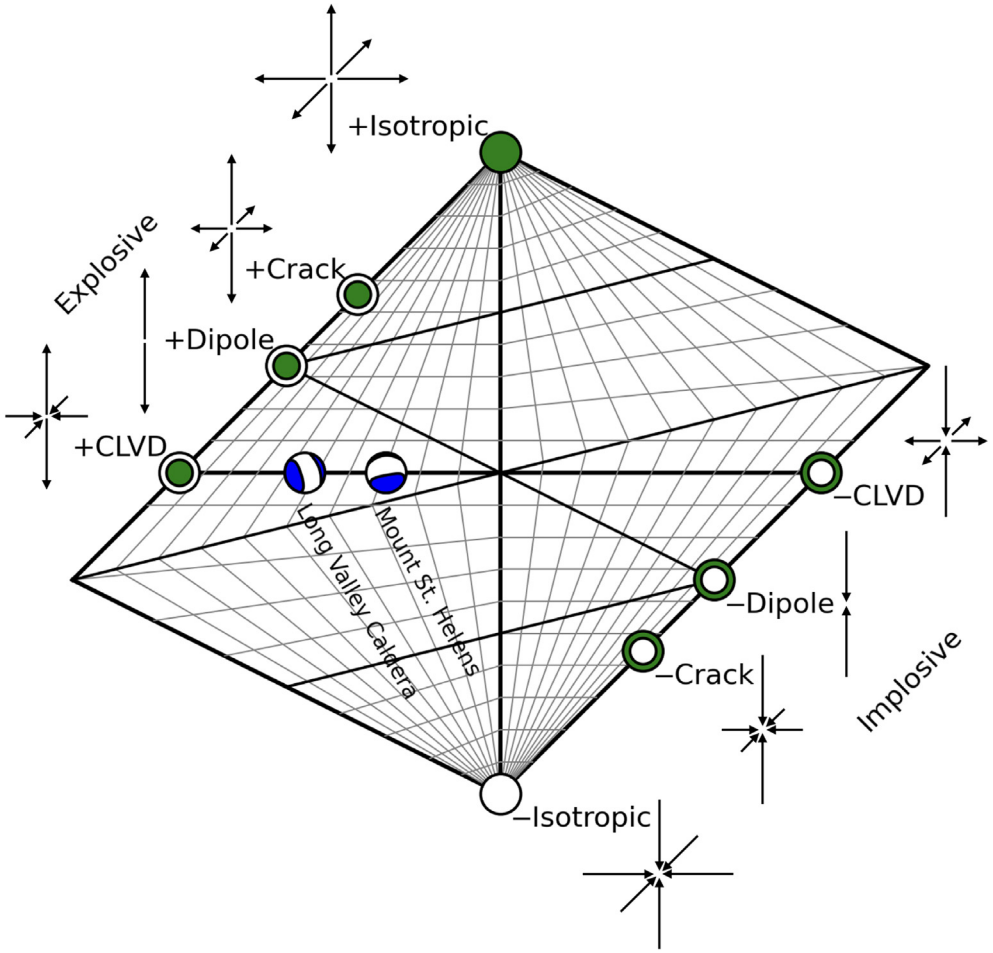

Figure 2. Source-type plot with force systems representing end members. Shown are the deviatoric moment tensors wherever present, which is the case for all but the fully isotropic source processes. Double-couple (DC) sources lie in the center of the plot, and the deviatoric moment tensors provided by the most moment tensor catalogs lie on its *x*-axis. Those source mechanisms allow for deformation at the source and thus compensated linear vector dipole (CLVD) components, but no volume change. The moment tensors of the 1980 Long Valley earthquake and Mount St. Helens eruption are shown as earthquakes with DC and CLVD components. The color version of this figure is available only in the electronic edition.

to be artifacts rather than reflecting true source processes. However, physical significance is often attributed to NDC components for earthquakes for which they are suggested by other (aftershocks, surface faulting, geodetic, etc.) data, or expected due to the geologic setting. In volcanic areas, whether to attribute NDC components to multiple faults or volcanic processes is sometimes unclear (Wallace, 1985), especially because the faulting and magmatism may be related (Minson *et al.*, 2007).

As a complement to studies of individual earthquakes, our approach in this article is to examine a large moment tensor dataset to assess how NDC components vary with earthquake magnitude, mechanism type, and geologic setting. This approach builds on an earlier study that used a large dataset to assess the uncertainties in the moment tensors and quantities derived from them (Rösler *et al.*, 2021).

Moment Tensor Dataset

We compile a dataset of NDC components by combining global and regional moment tensor catalogs for 2016–2020. The Global Centroid Moment Tensor (Global CMT) Project (Ekström *et al.*, 2012), U.S. Geological Survey (USGS), and Deutsches GeoForschungsZentrum (GFZ) catalogs provide moment tensors for a global distribution of earthquakes with differing minimum magnitudes. For consistency, we use moment tensors from these catalogs only for earthquakes with $M_w > 4.5$. The Global CMT, USGS, and GFZ catalogs contributed 11683, 4916, and 4751 source mechanisms to our dataset (Fig. 3a). For earthquakes with magnitude $M_w < 4.5$, we use four regional catalogs over the same time range. The Northern California Earthquake Data Center and Southern California Earthquake Data Center (Fig. 3b) catalogs, with minimum magnitudes of M_w 2.9 and 4.0, respectively, contribute 333 and 44 moment tensors. The Istituto Nazionale di Geofisica e Vulcanologia catalog for the Mediterranean and adjacent regions, and the Instituto Geográfico Nacional catalog for the Iberian peninsula contain 362 and 57 moment tensors with $M_w > 3.3$ (Fig. 3c), respectively.

For nearly all earthquakes with magnitude $M_w > 5.5$, several moment tensor solutions are available (Fig. 4a). To avoid bias in the calculation of the NDC component due to a larger number of points for larger earthquakes, we average over the elements of moment tensors for the same earthquake, identified in different catalogs by similar source times (± 60 s) and locations (difference less than 1°). Similar results arise from including the individual solutions as separate earthquakes.

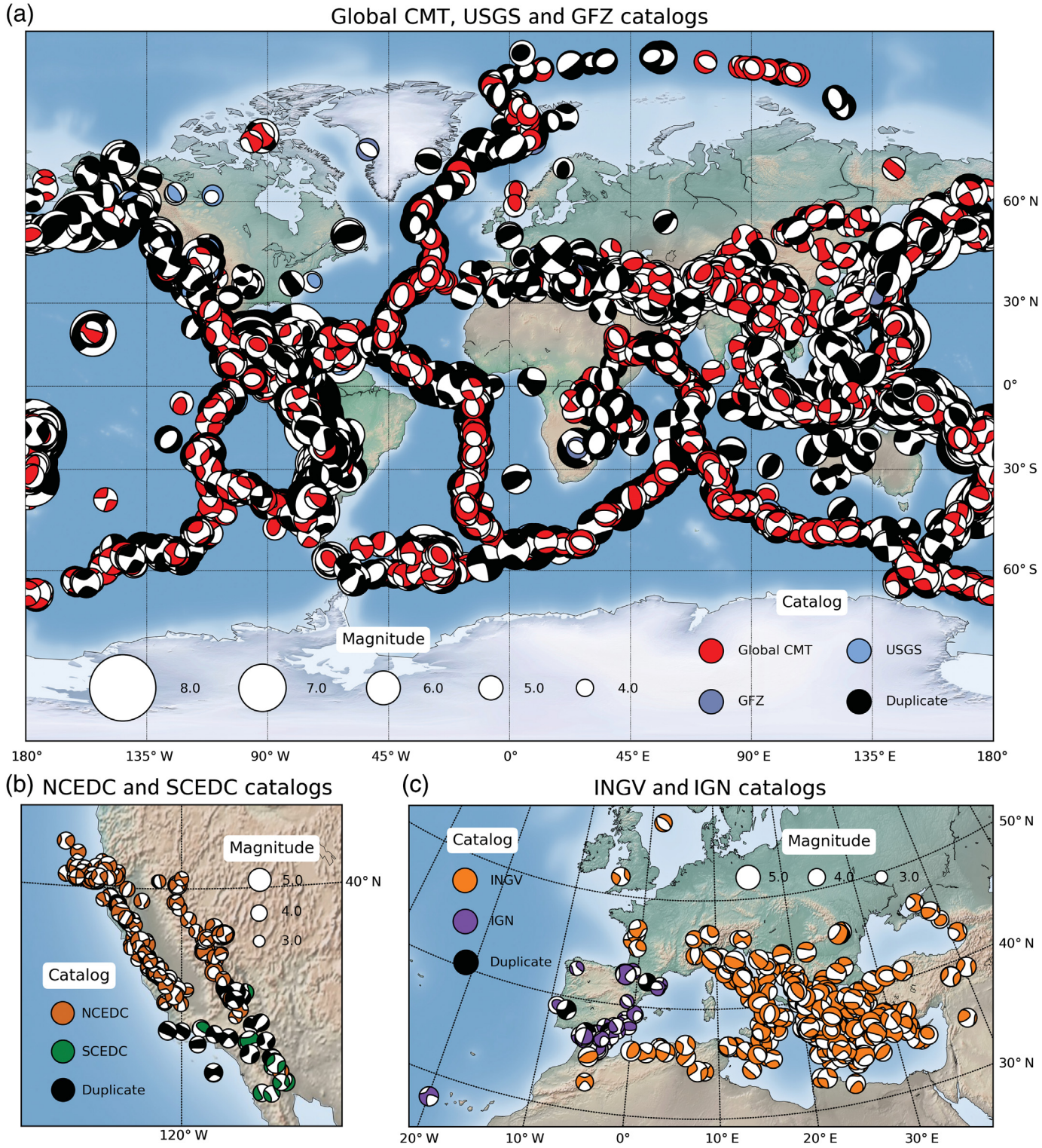

Figure 3. (a) Source mechanisms of $M_w > 4.5$ earthquakes from the Global Centroid Moment Tensor (Global CMT), U.S. Geological Survey (USGS), and GeoForschungsZentrum (GFZ) catalogs. Most earthquakes are duplicates between catalogs, but the Global CMT catalog contains some earthquakes for which other catalogs do not provide source mechanisms. (b,c) Source mechanisms of $M_w < 4.5$ earthquakes from Northern California Earthquake Data Center (NCEDC) and Southern California Earthquake Data Center (SCEDC), and The Istituto Nazionale di Geofisica e Vulcanologia (IGNV) and Instituto Geográfico Nacional (IGN) catalogs. Earthquakes occurring at the same time and the same location are considered duplicates.

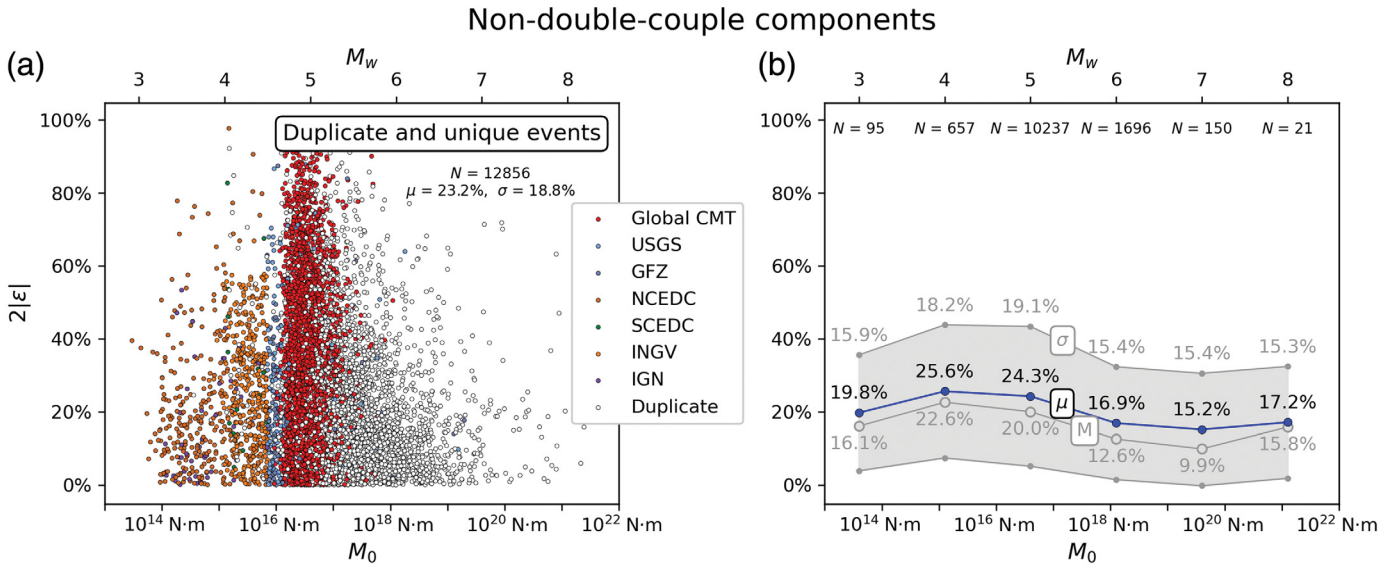

Figure 4. (a) NDC components in the global and regional moment tensor catalogs. Global and regional catalogs cover magnitudes with $M_w > 4.5$ and $M_w < 4.5$, respectively. Earthquakes unique to one catalog are marked in color, whereas those from multiple catalogs are marked in white. (b) The mean (μ) and median (M) NDC components for one magnitude unit bins are basically constant over this large magnitude range. Standard deviations (σ) are shown by shaded area and labeled values.

Consistency of NDC Components with Magnitude

Figure 4 shows the deviation from a double-couple source, $2|\epsilon|$, versus magnitude for the 12,856 earthquakes in our dataset, which covers a wide range of magnitudes and regions, and hence geologic environments. To illustrate the size of the NDC components, we consider their absolute values. The mean NDC component is 23.2%, consistent with the ~ 20% reported by Frohlich (1994). The average deviation from a DC source is essentially constant over this large magnitude range with only slight variations. The distributions of NDC components for different magnitude ranges overlap (Fig. 4), varying only slightly with magnitude. Although the differences between bins are formally significant, as shown by the standard errors of the mean (the standard deviation of the data divided by the square root of the number of data), the consistency is the primary characteristic of the data.

This observation could indicate that earthquakes are equally likely to rupture multiple faults across all magnitude ranges. However, Quigley *et al.* (2017) analyzed a large dataset of finite-fault rupture models for continental earthquakes with magnitude $4.1 < M_w < 8.1$ and found multifault rupture only for events with $M_w > 6.0$. Hence, larger earthquakes should be more likely to rupture multiple faults with different orientations and different slip directions than small earthquakes, yielding NDC components. Moreover, seismic waves excited by large earthquakes have lower frequencies than those of smaller earthquakes. As a result, slip on multiple faults in small earthquakes would not be revealed in a moment tensor inversion using seismic waves with frequencies lower than those present in the source. Therefore, a constant level of slip on multiple faults over all magnitudes should result in NDC components increasing with magnitude. Conversely, the consistency of NDC components with magnitude suggests that most NDC components do not reflect multiple rupture processes.

Considering the polarity of the smallest eigenvalue λ_3', the NDC components have a distribution that resembles a normal distribution (Fig. 5a). However, its heavy tails due to large NDC components with either polarity result in a kurtosis of 0.28 and a significant deviation from a normal distribution that causes the K^2 test (d'Agostino, 1971) to fail. The skewness of the distribution of 0.05 is negligible, indicating equal likelihood for positive and negative NDC components. The absolute NDC components (Fig. 5b) show that most earthquakes have small NDC components: 28.9% of all moment tensor solutions have NDC components of less than 10%. However, 10.5% have an NDC component of more than 50%, more than in a normal distribution. The distributions are similar for the different magnitude ranges (Fig. 5c,d).

Consistency of NDC Components with Mechanism Type and Geologic Environment

To assess possible differences in NDC components, we classify the earthquakes by their faulting type, following Frohlich (1992). We calculate the plunge of the P, N, and T axes from the eigenvectors of the moment tensors. An earthquake is considered a normal faulting earthquake if the plunge of its P axis satisfies $\sin^2 \delta_P \leq 2/3$ ($\delta_P \leq 54.75°$), strike slip if its N axis plunge exceeds 54.75°, and a thrust fault if its T axis plunge exceeds 54.75° (Saloor and Okal, 2018). Of the earthquakes

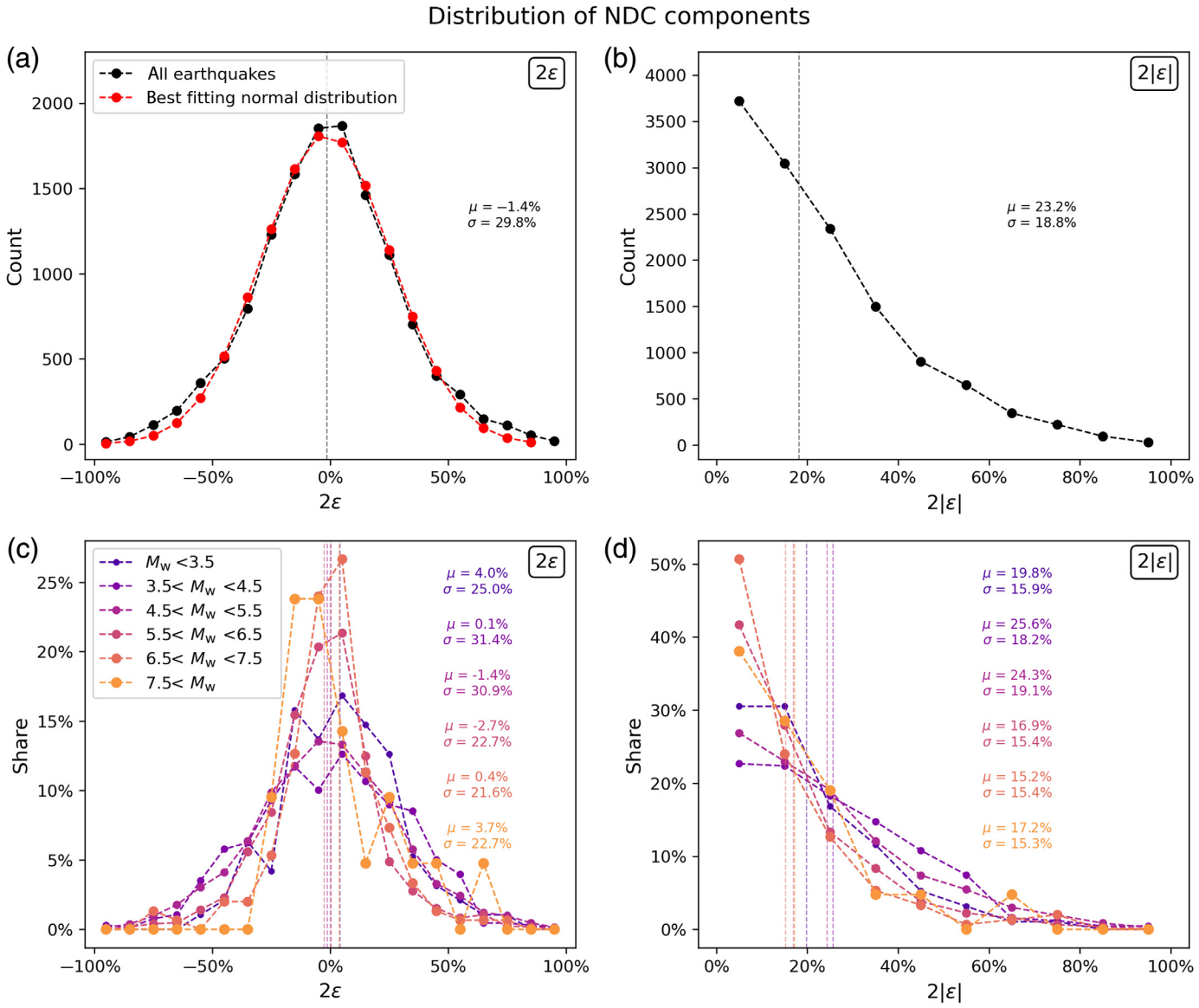

Figure 5. (a) Distribution of NDC components considering their polarity. Although the distribution closely resembles a normal distribution, it has heavier tails. (b) Distribution of absolute values of NDC components. Although most of the NDC components are small, 10.5% of earthquakes have NDC components exceeding 50%. (c,d) Distributions as in (a,b) for different magnitude bins. The color version of this figure is available only in the electronic edition.

in our study, 29.6% have thrust mechanisms, 29.8% are strike slip, and 24.7% have normal-faulting mechanisms. The plunge of none of the axes of the remaining 15.9% exceeds the threshold and are hence considered oblique faulting (Table 1a). Thrust-faulting events have the smallest NDC components, 18.1% on average. Strike-slip and normal-faulting earthquakes have similar NDC components of 25.2% and 25.5%, respectively. Oblique-faulting earthquakes do not differ, with a mean NDC component of 25.5%. Despite the slightly smaller NDC components for thrust earthquakes, the differences between earthquakes with different mechanisms are small and within one standard deviation.

Because of the large number of earthquakes in our dataset, the standard errors of the mean are small (Table 1a) and do not exceed 0.5% for earthquakes of any faulting type. Therefore, the smaller NDC components of thrust faults are statistically significant. This difference between faulting types is shown in the ternary diagram (Kaverina *et al.*, 1996) indicating slightly smaller NDC components for thrust faults than for other types of earthquakes (Fig. 6).

The polarities of the NDC components show some differences between fault types, as shown by their distributions. Strike-slip earthquakes tend to have more negative NDC components, whereas normal faulting earthquakes tend to have more positive NDC components (Fig. 7). A *t*-test reveals that the NDC components of the three types of earthquakes are from different distributions (Fig 7a). However, a *t*-test based on the

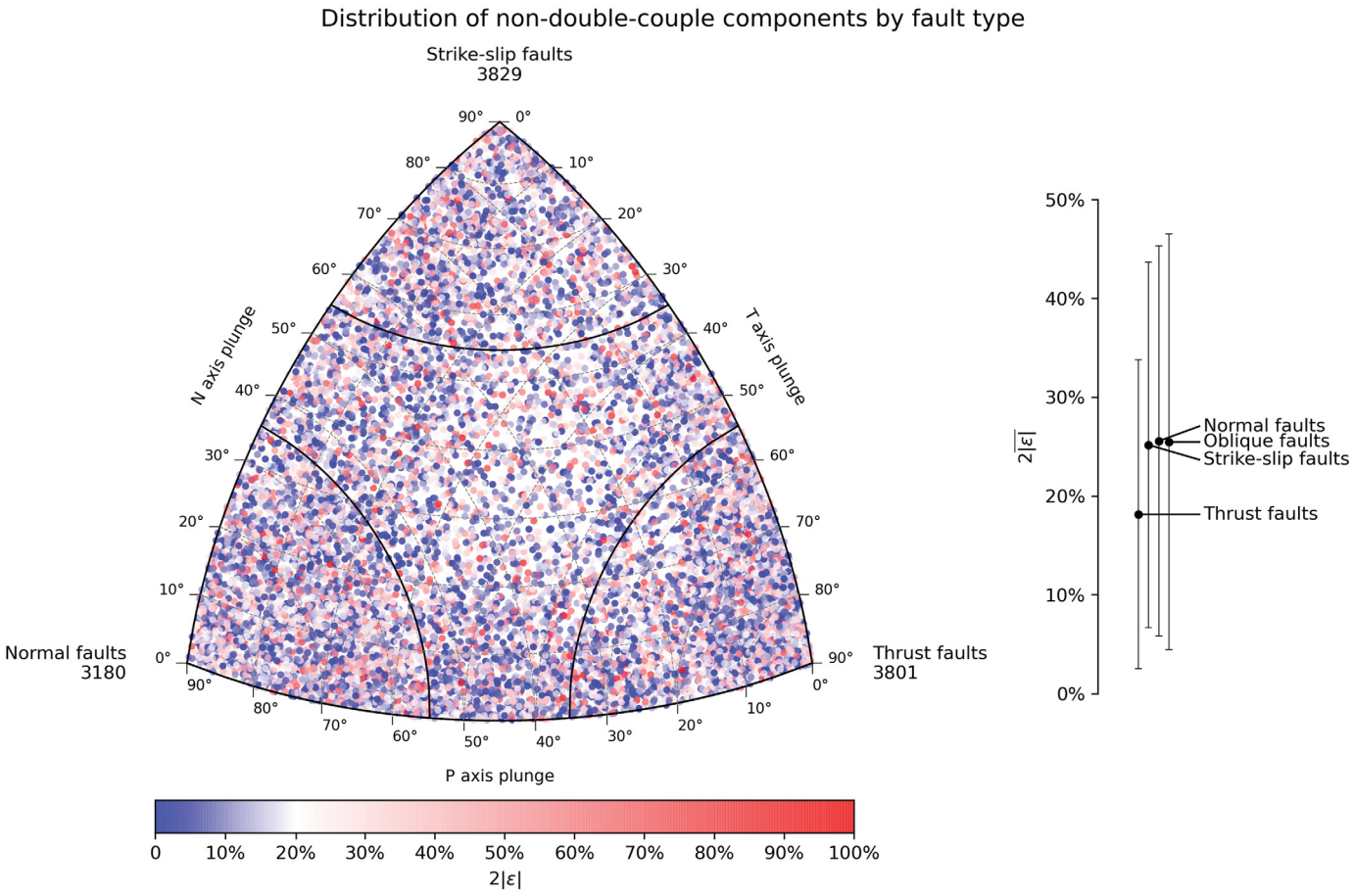

Figure 6. Distribution of NDC components by faulting type. The distribution of NDC components is similar between faulting types, with thrust events having slightly smaller NDC components.

TABLE 1
Mean Deviation (μ) from a Double-Couple (DC) Source of the Moment Tensors for Earthquakes Classified by Faulting Type and Geologic Environment, Standard Error of the Mean (σ_μ), and Standard Deviation (σ)

Complete Dataset	***N***	μ	σ_μ	σ
	12856	**23.2%**	**0.2%**	**18.8%**
(a) Faulting type				
Thrust	3801	18.1%	0.3%	15.6%
Strike-slip	3829	25.2%	0.3%	18.5%
Normal	3180	25.5%	0.4%	19.8%
Oblique	2046	25.5%	0.5%	21.0%
(b) Geologic environment				
Subduction zone	8691	21.6%	0.2%	19.7%
Spreading center	2785	28.0%	0.4%	18.2%
Volcanoes	163	26.0%	1.6%	20.0%

absolute values of the NDC components shows that strike-slip and normal-faulting earthquakes have the same distribution (p = 0.4). In addition, the cumulative density function shows that thrust-faulting earthquakes are more likely to have small NDC components than earthquakes with other faulting types (Fig. 7c). Whether these differences reflect real differences in fault behavior or artifacts of the inversion process is unclear.

Subduction zones host primarily thrust- and normal-faulting earthquakes, whereas spreading centers host normal-faulting and strike-slip events. Using the earthquakes' locations, we classify earthquakes by geologic environment (Fig. 8). Most earthquakes in our dataset occur in subduction zones (Fig. 8a), with a mean NDC component of 21.6% (Table 1b). This is slightly smaller than for earthquakes at spreading centers (Fig. 8b), which average 28.0%, and consistent with the observation that thrust-faulting earthquakes have slightly smaller NDC components than earthquakes of other faulting types (Table 1a). In our dataset, 3584 of 8691 earthquakes at subduction zones are thrust-faulting earthquakes, and 1742 have a normal-faulting mechanism. At spreading centers, normal- and strike-slip-faulting earthquakes constitute about an equal

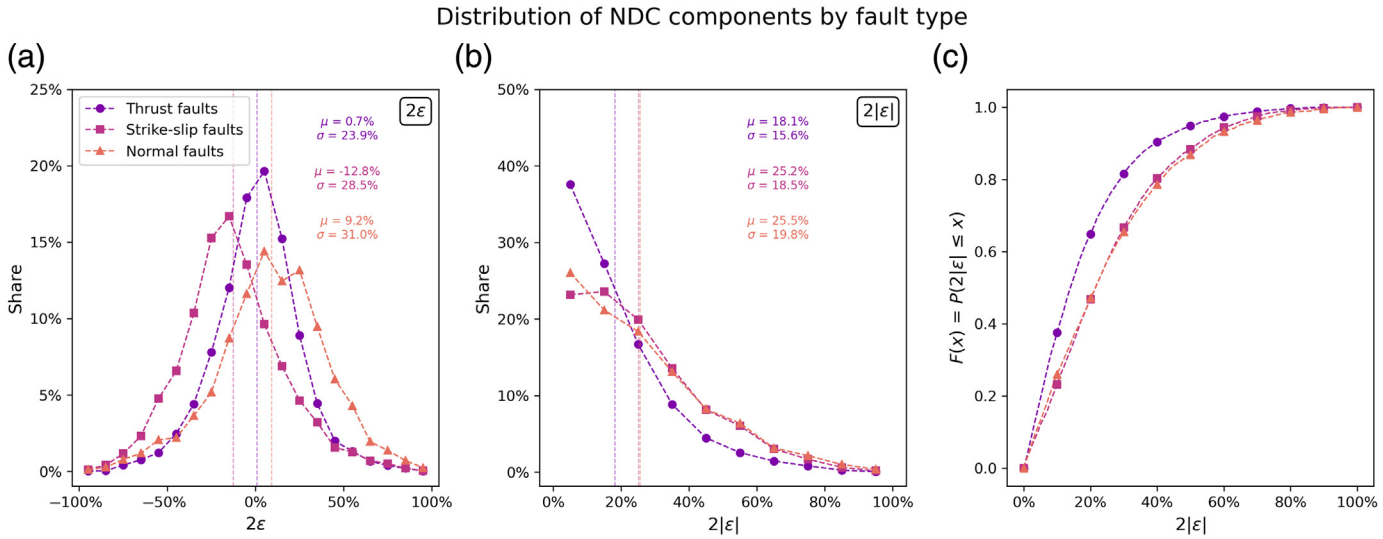

Figure 7. (a) Distribution of NDC components classified by faulting type. Strike-slip faults tend to have more negative NDC components than thrust faults, whereas normal faults tend to have more positive NDC components. (b) Distribution of absolute values of NDC components. Thrust faults have slightly smaller absolute NDC components than other fault types. However, this difference is too small to show a systematic relationship between faulting types and NDC components. (c) Cumulative distribution functions of the absolute values of NDC components of earthquakes with different faulting types. Thrust faults are more likely to have small NDC components than earthquakes with other faulting types. The color version of this figure is available only in the electronic edition.

share of the earthquakes observed at this geologic environment with 1132 and 1444 earthquakes, respectively. Earthquakes of both faulting types have nearly identical average NDC components.

To identify earthquakes possibly related to volcanism, we calculate the distance of each earthquake from the 1416 volcanoes with Holocene eruptions, roughly the last 10,000 yr (Global Volcanism Program, 2013). We classify an earthquake as volcanic if it occurred within 10 km of a volcano (Fig. 8c) and so may reflect magmatism, associated faulting, or a combination. The 163 volcanic earthquakes have an average NDC component of 26.0% (Table 1b), which is slightly larger but does not differ significantly from the remaining 12,693 earthquakes' value of 23.2%, and is smaller than earthquakes at spreading centers' value of 28.0%. Thus, although many well-known cases of NDC components occur in volcanic, hence extensional, settings, this effect seems not to be a primary cause of the pervasive ~ 20% NDC components observed.

The distribution of NDC components for earthquakes in different geologic environments are all approximately centered around zero (Fig. 9a). Slight asymmetries are shown by the skewness, defined as

$$\tilde{\mu}_3 = \frac{\sum_{i=1}^{N}(\epsilon_i - \mu)^3}{(N-1)\sigma^3}, \tag{5}$$

where μ and σ denote the mean and standard deviation of the distribution of NDC components, which is influenced more strongly by the tails of a distribution than by values close to the mean. The distribution for earthquakes at subduction zones most closely resembles a normal distribution with zero mean and $\tilde{\mu}_3 = -0.02$. The distributions for earthquakes at spreading centers are skewed to positive NDC components ($\tilde{\mu}_3 = 0.22$) and that for volcanic earthquakes is skewed to negative NDC components ($\tilde{\mu}_3 = -0.24$). The absolute value of NDC components (Fig. 9b) is smallest for earthquakes at subduction zones, whereas the heavier tails of NDC components at spreading centers result in slightly larger NDC components on average. Similarly, volcanic earthquakes have slightly larger NDC components on average.

Generation of NDC Components by Multifault Ruptures

NDC components of moment tensors can arise from near-simultaneous earthquakes on nearby faults with different geometries (Fig. 1b) (Hamling *et al.*, 2017; Ruhl *et al.*, 2021; Yang *et al.*, 2021) or portions of a rupture with changes in geometry (Cohee and Beroza, 1994; Wald and Heaton, 1994; Pang *et al.*, 2020).

To gain insight into the consistency of NDC components with magnitude and source type, we explore the effect of rupture on nearby faults with different geometry by modeling the sum of DC sources. Figure 10 shows the NDC component resulting from adding two DC sources. The similarity between the DC sources is characterized by the angle Φ needed to rotate one moment tensor's principal axes into the other (Kagan, 1991). As shown, the fault angles of the DC sources must be substantially different (rotation angles of more than 40°) to generate an NDC component exceeding the mean observed

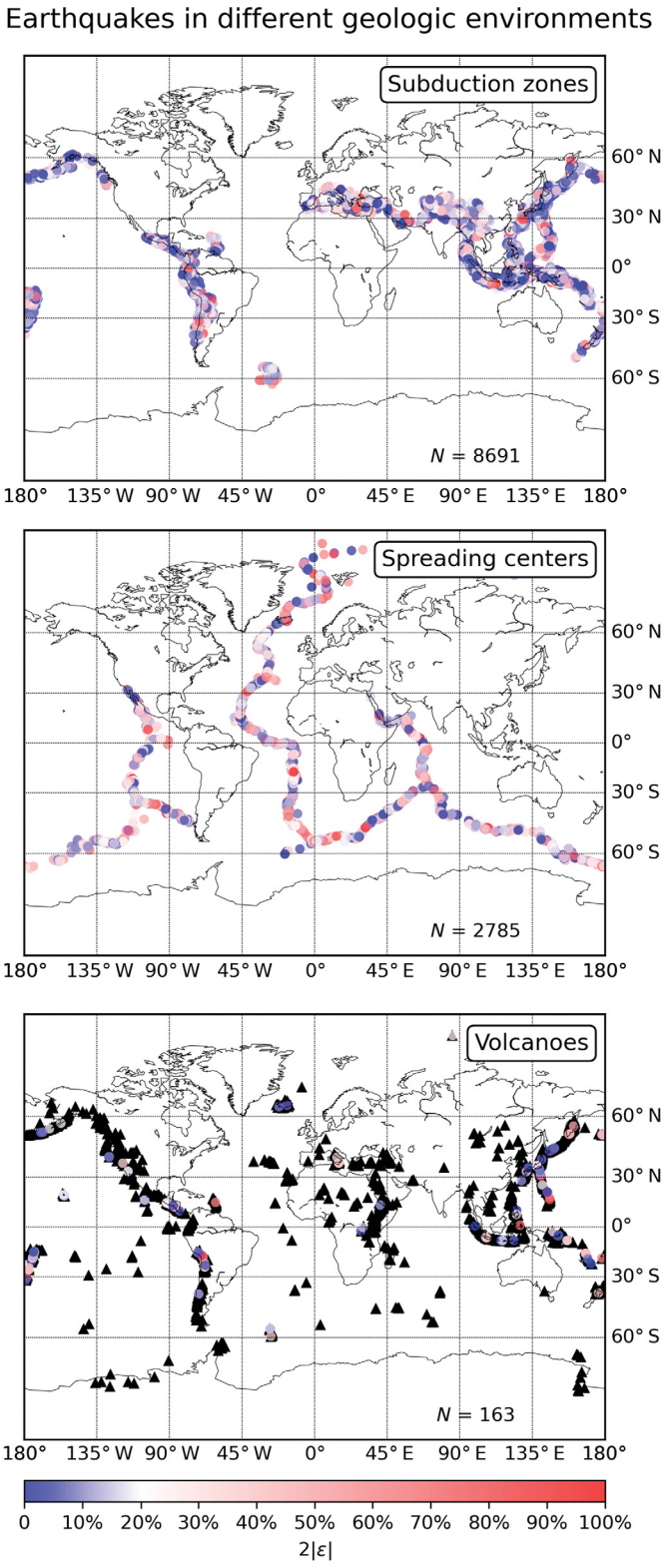

Figure 8. Location of earthquakes and magnitude of NDC components in different geologic environments. Subduction zones host primarily thrust and normal-faulting earthquakes, whereas spreading centers host normal-faulting and strike-slip events, which explains the slightly smaller NDC components at subduction zones. Volcanic areas are known to host earthquakes with complex source processes, resulting in slightly larger NDC components on average.

NDC component of 23.2%. This effect is illustrated by the two examples in Figure 1b. The 2016 Italy earthquake whose faults differ by a rotation angle of 56° yields an NDC component of 15%, whereas the 2020 Idaho earthquake with faults differing by 87° yields a larger 43% NDC component.

Although such large rotation angles often arise for large earthquakes that rupture several faults, we expect that such major changes in fault geometry should be rare for smaller earthquakes with simpler source processes. Thus, we consider it likely that NDC components of smaller earthquakes are primarily artifacts of the inversion.

We illustrate the mechanisms leading to significant NDC components by modeling a seismic source as the sum of an MDC and an mDC source with equal seismic moments. Figure 11 shows the absolute NDC components arising from adding an mDC to a strike-slip MDC (Fig. 11a–c) and a thrust fault MDC (Fig. 11d–f), when changing two of the three fault angles of the mDC source. For both types of MDC sources, the mechanism of the mDC source must be fundamentally different from the MDC source to generate a NDC component exceeding the average observed NDC component of 23.2%.

For the cases considered, large NDC components can arise for thrust-faulting events (and therefore normal-faulting events that have the same mechanism for the generation of NDC components) when the mDC differs from the MDC in only one fault angle, whereas strike-strike events require two angles to differ. Adding an mDC source that differs from the MDC in only one fault angle to a vertically dipping right-lateral strike-slip fault MDC striking North ($\Phi_f = 0°$, $\delta = 90°$, $\lambda = 180°$, Fig. 11a–c) does not create an NDC component. Therefore, we expect strike-slip-faulting events to have smaller NDC components. However, our dataset shows only small differences between strike-slip- and dip-slip-faulting earthquakes (Table 1a).

In contrast, for a 30°-dipping thrust fault ($\Phi_f = 0°$, $\delta = 30°$, $\lambda = 90°$), a variation in strike of the mDC component is necessary to generate a significant NDC component (Fig. 11d–f), whereas varying dip and slip angles alone do not lead to an NDC component. This is more likely to occur on the largest thrust fault events in subduction zones, where slip occurs over large distances, than for normal-faulting earthquakes. However, our dataset shows only small differences between thrust- and normal-faulting earthquakes (Table 1a).

Discussion and Conclusions

Previous studies of individual earthquakes have shown that NDC components may reflect components of the source beyond slip on a planar fault in specific geologic environments, notably volcanic areas, the combined effect of DC sources with different geometries, or artifacts of the inversion. Here, we take a complementary approach by examining a large moment tensor dataset to assess how NDC components vary with earthquake magnitude, mechanism type, and geologic environment. This approach gives insight into general

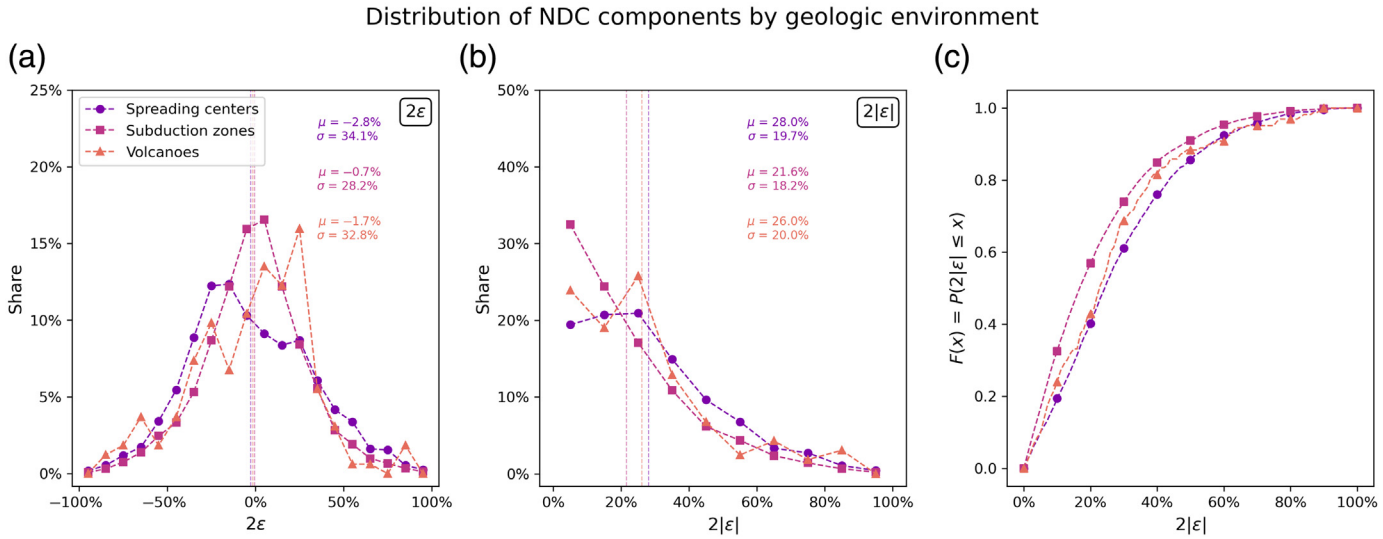

Figure 9. (a) Distribution of NDC components classified by geologic environment. The distribution for earthquakes at subduction zones resembles a normal distribution with zero mean, whereas the distribution for earthquakes at spreading centers is skewed to positive NDC components. The distribution for volcanic earthquakes is skewed to negative NDC components. (b) The mean absolute value of NDC components is the smallest for earthquakes at subduction zones, whereas the larger NDC components of earthquakes at spreading centers and at volcanoes are similar. (c) Cumulative distribution functions of the absolute values of NDC components in different geologic environments. Earthquakes in different geologic environments show similar distributions. The color version of this figure is available only in the electronic edition.

properties of the NDC components of many earthquakes. In the traditional formulation for inverse problems, our study gains high stability, identifying general properties of NDC components, at the cost of low resolution, specifics for individual earthquakes.

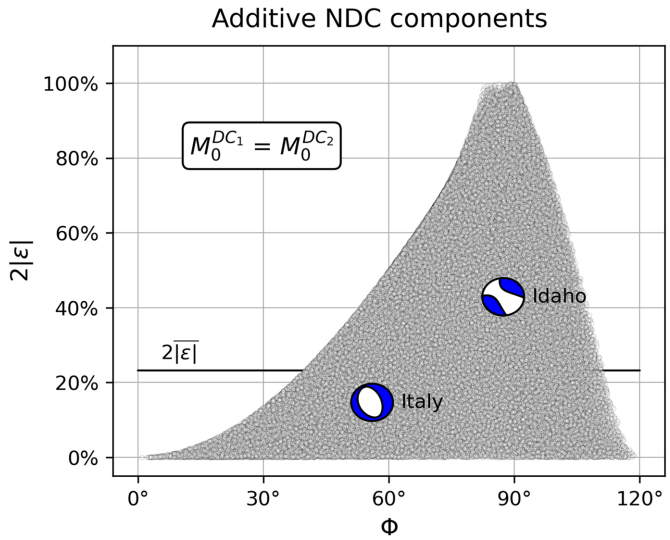

Figure 10. Difference between DC source mechanisms and resulting absolute NDC components. DC sources with substantially different source mechanisms, which are unlikely to occur for small earthquakes, are needed to exceed the mean observed NDC component of 23.2%. The color version of this figure is available only in the electronic edition.

The consistency of NDC components across a broad magnitude range suggests that most NDC components do not reflect rupture processes on multiple faults, which should have a greater effect for larger earthquakes, because a significant NDC component requires substantially different geometry between fault segments. Because multifault rupture has not been observed for smaller earthquakes, we discard an alternative interpretation that the consistency indicates that earthquakes of all magnitudes have equally complicated rupture processes. Furthermore, there are at most small differences in NDC components between earthquakes with different faulting mechanisms and in different geologic environments. This consistency suggests that most NDC components do not reflect actual source processes, which would likely cause variability. Hence, although some earthquakes have real NDC components, it appears that for most earthquakes, especially smaller ones, the NDC components are likely to be artifacts of the inversion.

Data and Resources

The moment tensors used in this study were compiled from publicly available data sets. Global Centroid Moment Tensor (Global CMT) solutions are from https://www.globalcmt.org. The U.S. Geological Survey (USGS) catalog was downloaded using the Python package ObsPy and its International Federation of Digital Seismograph Networks webservice client (May 2021). Although publicly available, a compilation of the GEOFON data of the GeoForschungsZentrum

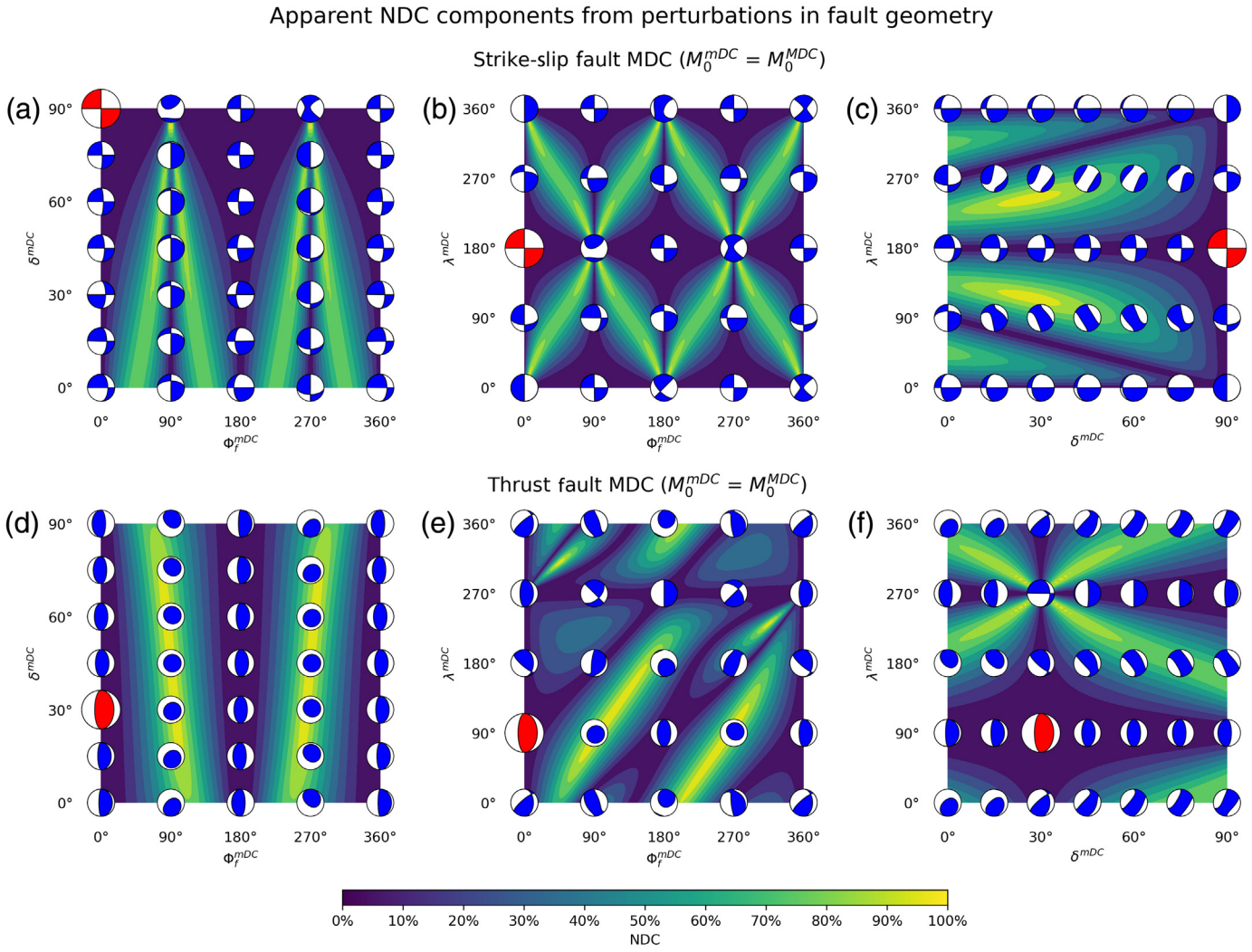

Figure 11. (a) Generation of NDC components due to adding a (a–c) minor double couple (mDC) source to a strike-slip major double couple (MDC) and (d–f) a thrust fault MDC. The MDC components are represented in red, and the moment tensors resulting from the combination of MDC and mDC components are shown in blue. In each subfigure, two fault angles of the mDC component are varied, whereas the third is the same as that of the MDC component. A difference in dip and slip angle between the MDC and mDC results in a large NDC component on a strike-slip MDC, whereas the variation of the strike angle is necessary to generate a significant NDC component at a thrust fault MDC. The color version of this figure is available only in the electronic edition.

(GFZ) German Research Centre for Geosciences was obtained through personal communication with Javier Quinteros (May 2021). Northern California Data Center (NCEDC) and Southern California Data Center (SCEDC) catalogs are available on https://ncedc.org and https://scedc.caltech.edu. Ellen Yu assisted in compiling the catalog of the SCEDC moment tensors. Catalogs of the Istituto Nazionale di Geofisica e Vulcanologia of Italy and the Instituto Geográfico Nacional of Spain (IGN) are available at https://ingv.it and https://www.ign.es. All websites were last accessed in May 2021. A list of the earthquakes used here including their moment tensors in different catalogs is available as the supplemental material.

Declaration of Competing Interests

The authors acknowledge that there are no conflicts of interest recorded.

Acknowledgments

The authors thank Emile Okal, Bruce Spencer, Susan Hough, Norman Abrahamson, and Craig Bina for helpful discussions. The article benefited from reviews by Honn Kao, Bruce Julian, and an anonymous reviewer. The authors thank Javier Quinteros for assistance with the GeoForschungsZentrum (GFZ) catalog and Ellen Yu for assistance with the Southern California Data Center (SCEDC) catalog. The authors thank Josó Antonio Álvarez Gómez for providing code in Python. This research was partially supported by the U.S. Geological Survey (USGS) Contract Number G19AC00104.

References

Ammon, C. J., T. Lay, A. A. Velasco, and J. E. Vidale (1994). Routine estimation of earthquake source complexity: The 18 October 1992 Colombian earthquake, *Bull. Seismol. Soc. Am.* **84,** no. 4, 1266–1271.

Cesca, S., E. Buforn, and T. Dahm (2006). Amplitude spectra moment tensor inversion of shallow earthquakes in Spain, *Geophys. J. Int.* **166,** no. 2, 839–854.

Chapman, M. C. (2013). On the rupture process of the 23 August 2011 Virginia earthquake, *Bull. Seismol. Soc. Am.* **103,** no. 2A, 613–628.

Cirella, A., A. Piatanesi, E. Tinti, M. Chini, and M. Cocco (2012). Complexity of the rupture process during the 2009 L'Aquila, Italy, earthquake, *Geophys. J. Int.* **190,** no. 1, 607–621.

Cohee, B. P., and G. C. Beroza (1994). Slip distribution of the 1992 Landers earthquake and its implications for earthquake source mechanics, *Bull. Seismol. Soc. Am.* **84,** no. 3, 692–712.

d'Agostino, R. B. (1971). An omnibus test of normality for moderate and large size samples, *Biometrika* **58,** no. 2, 341–348.

Domingues, A., S. Custodio, and S. Cesca (2013). Waveform inversion of small-to-moderate earthquakes located offshore southwest Iberia, *Geophys. J. Int.* **192,** no. 1, 248–259.

Dziewonski, A. M., and J. Woodhouse (1983). An experiment in systematic study of global seismicity: Centroid-moment tensor solutions for 201 moderate and large earthquakes of 1981, *J. Geophys. Res.* **88,** no. B4, 3247–3271.

Dziewonski, A. M., T. A. Chou, and J. H. Woodhouse (1981). Determination of earthquake source parameters from waveform data for studies of global and regional seismicity, *J. Geophys. Res.* **86,** no. B4, 2825–2852.

Ekström, G., M. Nettles, and A. Dziewonski (2012). The global CMT project 2004-2010: Centroid-moment tensors for 13,017 earthquakes, *Phys. Earth Planet. In.* **200–201,** 1–9.

Ford, S. R., D. S. Dreger, and W. R. Walter (2010). Network sensitivity solutions for regional moment-tensor inversions, *Bull. Seismol. Soc. Am.* **100,** no. 5A, 1962–1970.

Frohlich, C. (1992). Triangle diagrams: ternary graphs to display similarity and diversity of earthquake focal mechanisms, *Phys. Earth Planet. In.* **75,** nos. 1/3, 193–198.

Frohlich, C. (1994). Earthquakes with non-double-couple mechanisms, *Science* **264,** no. 5160, 804–809.

Gilbert, F. (1971). Excitation of the normal modes of the earth by earthquake sources, *Geophys. J. Int.* **22,** no. 2, 223–226.

Global Volcanism Program (2013). *Volcanoes of the World, v. 4.10.2*, in Venzke, E. (Editor), Smithsonian Institution, Washington, D.C., Downloaded 10 Sept. 2021, doi: 10.5479/si.GVP.VOTW4-2013.

Hamling, I. J., S. Hreinsdóttir, K. Clark, J. Elliott, C. Liang, E. Fielding, P. Villamor, L. Wallace, T. J. Wright, E. D'Anastasio, *et al.* (2017). Complex multifault rupture during the 2016 Mw 7.8 Kaikōura earthquake, New Zealand, *Science* **356,** no. 6334, doi: 10.1126/science.aam7194.

Hayes, G. P., R. W. Briggs, A. Sladen, E. J. Fielding, C. Prentice, K. Hudnut, P. Mann, F. W. Taylor, A. J. Crone, R. Gold, *et al.* (2010). Complex rupture during the 12 January 2010 Haiti earthquake, *Nature Geosci.* **3,** no. 11, 800–805.

Hudson, J. A., R. G. Pearce, and R. M. Rogers (1989). Source type plot for inversion of the moment tensor, *J. Geophys. Res.* **94,** no. B1, 765–774.

Jechumtálová, Z., and J. Šílený (2001). Point-source parameters from noisy waveforms: Error estimate by Monte-Carlo simulation, *Pure Appl. Geophys.* **158,** no. 9, 1639–1654.

Julian, B. R. (1983). Evidence for Dyke intrusion earthquake mechanisms near Long Valley caldera, California, *Nature* **303,** no. 5915, 323–325.

Julian, B. R., and S. A. Sipkin (1985). Earthquake processes in the Long Valley caldera area, California, *J. Geophys. Res.* **90,** no. B13, 11,155–11,169.

Julian, B. R., A. D. Miller, and G. R. Foulger (1998). Non-double-couple earthquakes 1. Theory, *Rev. Geophys.* **36,** no. 4, 525–549.

Kagan, Y. Y. (1991). 3-D rotation of double-couple earthquake sources, *Geophys. J. Int.* **106,** no. 3, 709–716.

Kanamori, H., and J. W. Given (1981). Use of long-period surface waves for rapid determination of earthquake-source parameters, *Phys. Earth Planet. In.* **27,** no. 1, 8–31.

Kanamori, H., and J. W. Given (1982). Analysis of long-period seismic waves excited by the May 18, 1980, eruption of Mount St. Helens–A terrestrial monopole? *J. Geophys. Res.* **87,** no. B7, 5422–5432.

Kaverina, A. N., A. V. Lander, and A. G. Prozorov (1996). Global creepex distribution and its relation to earthquake-source geometry and tectonic origin, *Geophys. J. Int.* **125,** no. 1, 249–265.

Kawakatsu, H. (1991). Enigma of earthquakes at ridge-transform-fault plate boundaries distribution of non-double couple parameter of Harvard CMT Solutions, *Geophys. Res. Lett.* **18,** no. 6, 1103–1106.

Knopoff, L., and M. J. Randall (1970). The compensated linear-vector dipole: A possible mechanism for deep earthquakes, *J. Geophys. Res.* **75,** no. 26, 4957–4963.

McNamara, D. E., H. M. Benz, R. B. Herrmann, E. A. Bergman, P. Earle, A. Meltzer, M. Withers, and M. Chapman (2014). The Mw 5.8 Mineral, Virginia, earthquake of August 2011 and aftershock sequence: Constraints on earthquake source parameters and fault geometry, *Bull. Seismol. Soc. Am.* **104,** no. 1, 40–54.

Miller, A. D., G. R. Foulger, and B. R. Julian (1998). Non-double-couple earthquakes 2. Observations, *Rev. Geophys.* **36,** no. 4, 551–568.

Minson, S. E., D. S. Dreger, R. Bürgmann, H. Kanamori, and K. M. Larson (2007). Seismically and geodetically determined non-double-couple source mechanisms from the 2000 Miyakejima volcanic earthquake swarm, *J. Geophys. Res.* **112,** no. B10, doi: 10.1029/2006JB004847.

Nettles, M., and G. Ekström (1998). Faulting mechanism of anomalous earthquakes near Bárdarbunga volcano, Iceland, *J. Geophys. Res.* **103,** no. B8, 17,973–17,983.

Pang, G., K. D. Koper, M. Mesimeri, K. L. Pankow, B. Baker, J. Farrell, J. Holt, J. M. Hale, P. Roberson, R. Burlacu, *et al.* (2020). Seismic analysis of the 2020 Magna, Utah, earthquake sequence: Evidence for a Listric Wasatch fault, *Geophys. Res. Lett.* **47,** no. 18, doi: 10.1029/2020GL089798.

Quigley, M. C., H. Mohammadi, and B. G. Duffy (2017). Multi-fault earthquakes with kinematic and geometric rupture complexity: How common? *INQUA Focus Group Earthquake Geology and Seismic Hazards*, New Zealand, 13–16 November.

Rößler, D., F. Krüger, and G. Rümpker (2007). Retrieval of moment tensors due to dislocation point sources in anisotropic media using standard techniques, *Geophys. J. Int.* **169,** no. 1, 136–148.

Rösler, B., S. Stein, and B. D. Spencer (2021). Uncertainties in seismic moment tensors inferred from differences between global

catalogs, *Seismol. Res. Lett.* **92,** no. 6, 3698–3711 doi: 10.1785/0220210066.

Ruhl, C. J., E. A. Morton, J. M. Bormann, R. Hatch-Ibarra, G. Ichinose, and K. D. Smith (2021). Complex fault geometry of the 2020 Mww 6.5 Monte Cristo Range, Nevada, earthquake sequence, *Seismol. Res. Lett.* **92,** no. 3, 1876–1890.

Saloor, N., and E. A. Okal (2018). Extension of the energy-to-moment parameter θ to intermediate and deep earthquakes, *Phys. Earth Planet. In.* **274,** 37–48.

Scognamiglio, L., E. Tinti, E. Casarotti, S. Pucci, F. Villani, M. Cocco, F. Magnoni, A. Michelini, and D. Dreger (2018). Complex fault geometry and rupture dynamics of the Mw 6.5, 30 October 2016, Central Italy earthquake, *J. Geophys. Res.* **123,** nos. 4, 2943–2964.

Šílený, J. (2004). Regional moment tensor uncertainty due to mismodeling of the crust, *Tectonophysics* **383,** nos. 3/4, 133–147.

Šílený, J., P. Campus, and G. F. Panza (1996). Seismic moment tensor resolution by waveform inversion of a few local noisy records–I. Synthetic tests, *Geophys. J. Int.* **126,** no. 3, 605–619.

Sipkin, S. A. (1986). Interpretation of non-double-couple earthquake mechanisms derived from moment tensor inversion, *J. Geophys. Res.* **91,** no. B1, 531–547.

Tréhu, A. M., J. L. Nábělek, and S. C. Solomon (1981). Source characterization of two Reykjanes Ridge earthquakes: Surface waves and moment tensors; P waveforms and nonorthogonal nodal planes, *J. Geophys. Res.* **86,** no. B3, 1701–1724.

Vera Rodriguez, I., Y. J. Gu, and M. D. Sacchi (2011). Resolution of seismic-moment tensor inversions from a single array of receivers, *Bull. Seismol. Soc. Am.* **101,** no. 6, 2634–2642.

Wald, D. J., and T. H. Heaton (1994). Spatial and temporal distribution of slip for the 1992 Landers, California, earthquake, *Bull. Seismol. Soc. Am.* **84,** no. 3, 668–691.

Wallace, T. (1985). A reexamination of the moment tensor solutions of the 1980 Mammoth Lakes earthquakes, *J. Geophys. Res.* **90,** no. B13, 11,171–11,176.

Yang, J., H. Zhu, T. Lay, Y. Niu, L. Ye, Z. Lu, B. Luo, H. Kanamori, J. Huang, and Z. Li (2021). Multi-fault opposing-dip strike-slip and normal-fault rupture during the 2020 Mw 6.5 Stanley, Idaho earthquake, *Geophys. Res. Lett.* **48,** no. 10, doi: 10.1029/2021GL092510.

Manuscript received 12 July 2021
Published online 16 February 2022